AD-A190 515 NONDESTRUCTIVE MOISTURE MEASUREMENT IN MICROELECTRONICS 1/1
(U) CLARKSON UNIV POTSDAM NY DIV OF RESEARCH
D KANE ET AL. DEC 87 RADC-TR-87-210 F30602-81-C-0206
UNCLASSIFIED F/G 14/2 NL

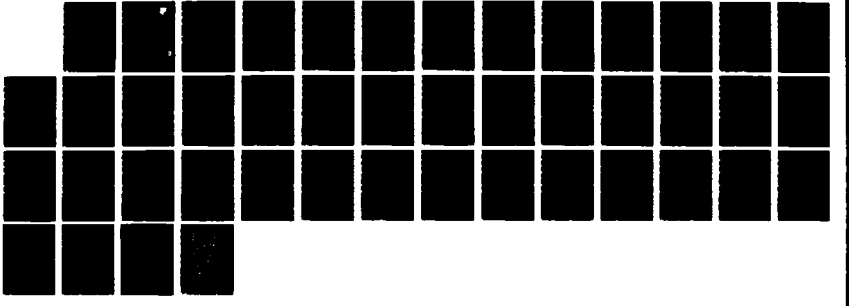

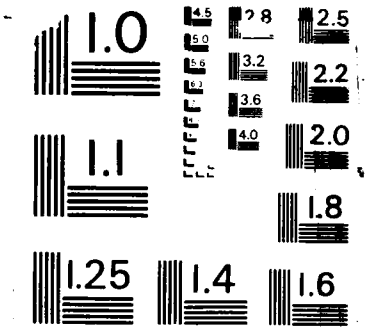

MICROCOPY RESOLUTION TEST CHART

NATIONAL BUREAU OF STANDARDS-1963-A

RADC-TR-87-210
Final Technical Report
November 1987

NONDESTRUCTIVE MOISTURE MEASUREMENT IN MICROELECTRONICS

Clarkson University

Didier Kane and Henry Domingos

ROME AIR DEVELOPMENT CENTER
Air Force Systems Command
Griffiss Air Force Base, NY 13441-5700

This report has been reviewed by the RADC Public Affairs Office (PA) and is releasable to the National Technical Information Service (NTIS). At NTIS it will be releasable to the general public, including foreign nations.

RADC-TR-87-210 has been reviewed and is approved for publication.

APPROVED: Benjamin A. Moore

BENJAMIN A. MOORE
Project Engineer

APPROVED: John J. Bart

JOHN J. BART
Technical Director
Directorate of Reliability & Compatibility

FOR THE COMMANDER: John A. Ritz

JOHN A. RITZ
Directorate of Plans & Programs

If your address has changed or if you wish to be removed from the RADC mailing list, or if the addressee is no longer employed by your organization, please notify RADC (RBRE) Griffiss AFB NY 13441-5700. This will assist us in maintaining a current mailing list.

Do not return copies of this report unless contractual obligations or notices on a specific document require that it be returned.

UNCLASSIFIED

SECURITY CLASSIFICATION OF THIS PAGE

REPORT DOCUMENTATION PAGE

Form Approved OMB No. 0704-0188

AD-A190 512

1a. REPORT SECURITY CLASSIFICATION UNCLASSIFIED	1b. RESTRICTIVE MARKINGS N/A
2a. SECURITY CLASSIFICATION AUTHORITY N/A	3. DISTRIBUTION / AVAILABILITY OF REPORT Approved for public release; distribution unlimited.
2b. DECLASSIFICATION / DOWNGRADING SCHEDULE N/A	
4. PERFORMING ORGANIZATION REPORT NUMBER(S) 4	5. MONITORING ORGANIZATION REPORT NUMBER(S) RADC-TR-87-210
6a. NAME OF PERFORMING ORGANIZATION Clarkson University 6b. OFFICE SYMBOL (If applicable)	7a. NAME OF MONITORING ORGANIZATION Rome Air Development Center (RBRE)
6c. ADDRESS (City, State, and ZIP Code) Division of Research 145 Clarkson Hall Potsdam NY 13676	7b. ADDRESS (City, State, and ZIP Code) Griffiss AFB NY 13441-5700
8a. NAME OF FUNDING / SPONSORING ORGANIZATION Rome Air Development Center 8b. OFFICE SYMBOL (If applicable) RBRE	9. PROCUREMENT INSTRUMENT IDENTIFICATION NUMBER F30602-81-C-0206
8c. ADDRESS (City, State, and ZIP Code) Griffiss AFB NY 13441-5700	10. SOURCE OF FUNDING NUMBERS PROGRAM ELEMENT NO: 61102F; PROJECT NO: 2306; TASK NO: J4; WORK UNIT ACCESSION NO: PJ

11. TITLE (Include Security Classification)
NONDESTRUCTIVE MOISTURE MEASUREMENT IN MICROELECTRONICS

12. PERSONAL AUTHOR(S)
Didier Kane, Henry Domingos

13a. TYPE OF REPORT	13b. TIME COVERED	14. DATE OF REPORT (Year, Month, Day)	15. PAGE COUNT
Final	FROM Sep 85 TO Aug 86	December 1987	48

16. SUPPLEMENTARY NOTATION
N/A

17. COSATI CODES			18. SUBJECT TERMS (Continue on reverse if necessary and identify by block number)
FIELD	GROUP	SUB-GROUP	Moisture, surface conductivity sensor, nondestructive measurements, adsorption physical models
14	04		
09	01		

19. ABSTRACT (Continue on reverse if necessary and identify by block number)

This project was aimed at understanding moisture induced effects on materials used in microelectronic device manufacture. The approach chosen has been the use of state-of-the-art interdigitated surface conductivity test structures for characterizing the responses of microelectronic materials to ambient and condensed moisture, by performing nondestructive moisture measurements on both hermetically sealed and delidded packages.

A test chamber and an appropriate electrical test setup have been developed for assessing the specificity, reproducibility and sensitivity of these effects.

Some physical models have been developed to determine and quantify the effect of adsorption and the sensitivity limit of this method, which allows recommending those approaches which would be most viable for adaptation to microelectronic processing.

20. DISTRIBUTION / AVAILABILITY OF ABSTRACT ☐ UNCLASSIFIED/UNLIMITED ☒ SAME AS RPT ☐ DTIC USERS	21. ABSTRACT SECURITY CLASSIFICATION UNCLASSIFIED
22a. NAME OF RESPONSIBLE INDIVIDUAL Benjamin A. Moore	22b. TELEPHONE (Include Area Code) (315) 330-4055 22c. OFFICE SYMBOL RADC (RBRE)

DD Form 1473, JUN 86 *Previous editions are obsolete*

SECURITY CLASSIFICATION OF THIS PAGE

UNCLASSIFIED

EVALUATION

The objective of this effort was to develop an understanding of moisture induced effects on materials used in microelectronic device manufacture and to then use this data to characterize the surface conductivity moisture sensor. This moisture sensing method was then evaluated for the purposes of optimizing sensitivity, decreasing hysteresis effects, determining detectability limits, and interpeting the moisture measurements. Theoretical and empirical models describing the physical reasons for differences between mass spectrometric moisture measurements at 100C and surface conductivity measurements at the condensation point were developed. These results will assist in evaluating the viability of the surface conductivity moisture sensor as a low cost, non-destructive alternative to mass spectrometric moisture determinations. These devices could be built into VLSI, VHSIC, and hybrid devices whose cost, complexity, and application demand a continuing reliability assessment.

The first part of the report discusses various moisture induced failure modes such as anodic and cathodic aluminum corrosion, metal migration, and instabilities, surface leakage, and surface inversions in MOS devices. The paper then gives a good discussion of state of the art surface conductivity moisture sensors and the development of a test chamber used to evaluate them. The discussion of the electrical measurement circuit describes a major improvement in the measurement technique that was developed during this effort.

In the past, surface conductivity moisture sensors have shown non-reproducible electrical response when mounted in packages and exposed to thermal cycling under DC bias. This is the result of variations in the silicon oxide upper layers, starting with nearly pure silicon oxide and becoming more and more a silico-aluminate with a constantly growing proportion of alumina reversibly changing from crystallites to gel with different time constants. Dr. Kane solved this problem by using a lock-in amplifier (LIA) whose internal generator was used for biasing the device under test (DUT) with a low voltage AC signal. Maximizing sensitivity of the measurement was accomplished by optimizing the LIA controls to provide the best signal to noise ratio. By using a high working frequency, the 1/f noise problem was minimized giving a clean signal for recording.

Successful results were obtained with AC biased sensors eutectically mounted on delidded TO cans and exposed to various controlled atmospheres. Important results were obtained in a series of experiments studying the sensor response to a wide range of known dew-frost points. A limit of approximately -25C below which no conduction can be detected was experimentally determined confirming a physical model developed during this study. These experiments also demonstrated the importance of having a diode integrated into the sensor chip to accurately measure the sensor temperature.

This work has successfully developed a new, original test setup at RADC. Calibrations have been performed on AC biased interdigitated surface conductivity moisture sensors in the range of 0C to -25C "dew-frost" points. A physical model has been developed which demonstrates that the sensitivity of these sensors could be improved by using an oxide with smaller pores. A copy of the final report will be forwarded to Harris Corporation, a manufacturer of these sensors who cooperated in this effort by providing evaluation samples. Looking to the future, a physical model that has been developed that allows correlating the electrical "dewpoint" measured by an in-situ surface conductivity sensor to the moisture content as measured by a mass spectrometer. Work is currently underway in-house to confirm this model.

BENJAMIN A. MOORE
Project Engineer

TABLE OF CONTENTS

List of Figures

List of Tables

I. INTRODUCTION

This project was aimed at understanding moisture induced effects on materials in microelectronic device manufacture. The approach chosen has been the use of state-of-the-art interdigited surface conductivity test structures for characterizing the responses of microelectronic materials to ambient and condensed moisture, by performing non-destructive moisture measurements on both hermetically sealed and delidded packages.

A test chamber and an appropriate electrical test setup have been developed for assessing the specificity, reproducibility and sensitivity of these effects.

Some physical models have been developed to determine and quantify the effect of adsorption and the sensitivity limit of this method, which allows recommending those approaches which would be most viable for adaptation to microelectronic processing.

II. HISTORICAL BACKGROUND

It has been a long time since the first awareness of the incidence of a component environment on its performance:

In 1955, Bergsten and McDowell described a mass spectrometer aimed at analyzing gaseous species in the internal atmosphere of a relay encapsulation. Since t..at moment, the reliability of a package has been considered to depend upon both hermeticity and internal atmosphere.

In 1966, P.H. Eisenberg showed that low temperature malfunctioning of some transistors and aluminum corrosion were due to the presence of moisture in the packages.

In the 70's, W.F. Keenon and W.R. Rungan reported moisture related corrosion failures on thin film nichrome resistors. These failures had escaped detection at the manufacturing plant, incoming inspection, electrical tests and burn-in tests. Failure analysis on these parts revealed pin-holes on the metallizations due to the combined effect of moisture, bias voltage and defects in the glassivation layer. As a response to these problems most manufacturers started to improve the quality of their glassivations, to use dry high temperature sealing processes and to impose biased thermal cycling tests.

At the same period, moisture had also been associated with electrical shorts by gold dendrites on hybrid modules.

In the early 80's, one of the big moisture related concerns was sealing glasses for cerdip packages. Devitrifying sealing glasses had a tendency to free some water molecules initially fixed in the PbO-B203 matrix, because of the nucleation around ZnO during the devitrification and have progressively been replaced by vitreous glasses.

Nowadays, the situation is even more challenging with the increasing use of organics in VLSI and hybrid packages, and with the growing flow of plastic packages on the market, for which diffusion of moisture through the materials involved has to be taken into account on top of adsorption, desorption, and absorption problems.

ALUMINUM CORROSION

Aluminum can be attacked by halogens cations such as F^-, Cl^-, Br^-, I^{--}, or by metal anions such as Cu^{++}, Na^+, K^+ . . . . . In order to prevent the diffusion of these ions, 1 to 4% copper is often added to the aluminum metallizations.

The corrosion mechanisms come from the biased metallizations acting as electrodes, and the adsorbed water and ionic impurities which create an electrolytic bath. Aluminum being amphoteric can react either anodically or cathodically.

CATHODIC CORROSION

This mechanism involves Na^+ or K^+ ions which, under the bias voltage, occupy vacant sites on the cathode (i.e. defects on surface of the aluminum):

$$Na^+ + e^- \rightarrow Na$$

$$Na + H_2O \rightarrow Na^+ + OH^- + H^+ e^-$$

$$4(OH)^- + Al \rightarrow Al\,(OH)^-_4 + 3e^-$$

$$Al(OH)^-_4 \rightarrow Al\,(OH)_3 + OH^-$$

The precipitated $Al(OH)_3$ forms a plug that isolates the electrolytic solution in the pit from the bulk solution, hence allowing the pit to grow.

ANODIC CORROSION

In this process, cations (Cl^-, S^- . . .) migrate under the bias potential to active sites in the native aluminum oxide Al_2O_3:

$$Al + 4\,Cl^- \rightarrow Al(Cl)^-_4 + 3e^-$$

$$Al(Cl)^-_4 + 3\,H_2O \rightarrow Al(OH)_3 + 6\,H^+ + 4\,Cl^- + 3e^-$$

$$Al + 3\,OH^- \rightarrow Al(OH)_3 + 3e^-$$

$$Al(OH)_3 + OH^- \rightarrow Al(OH)^-_4$$

Phosphoric acid can also be created from the phosphorus of the glassivation layer:

$$P_2O_5 + 3\,H_2O \rightarrow 2\,H_3PO_4$$

$$H_3PO_4 \rightarrow H_2PO^-_4 + H^+$$

$$H_2PO^-_4 \rightarrow H\,PO^{--}_4 + H^+$$

$$HPO^{--}_4 \rightarrow PO^{3-}_4 + H^+$$

Phosphates can also be formed. The resulting electrons can break the water molecules, releasing some OH groups which attack the aluminum instantaneously.

The PH in the pits depends upon the character, acid or basic, of the ions that migrate.

METAL MIGRATION

The most common moisture induced metal migration example are gold dendrite growth in hybrid devices, and silver migration on silver plated leads in resin-molded packages.

The treshold for these mechanisms has been shown to depend on relative humidity, the type and concentration of impurities, and the bias voltage applied (more precisely, the electrical field, which depends on the metallization spacing).

The failure mode is a short between two metal lines. It is strongly influenced by other factors such as the surface/volume ratio of the package, the operating temperature...

In the case of silver migration, when a dc bias is applied to the silver electrodes, silver dissolves at the anode as Ag^+. These Ag^+ ions combine with OH^- ions to form AgOH, which is unstable and changes to Ag_2O (a precipitate, easily reduced to metal Ag by the reducing materials contained in the insulating material). This precipitate is in a dendritic form.

INSTABILITIES, SURFACE LEAKAGE AND SURFACE INVERSIONS ON MOS DEVICES

Moisture can be responsible for electrical instabilities and surface inversions on MOS devices.

The most common moisture induced instability is a shift in the threshold voltage, which is the minimum voltage required to create a surface inversion channel in silicon. This generally occurs in negative bias conditions. It has been shown that the water and the hydrogen ions diffusing out of the phosphosilicate glass passivation layer are mainly responsible for this instability phenomenon.

Even though the mechanism itself is not well understood at this time, it is suspected that a large positive charge builds up near the source (and drain, depending on the bias conditions) area(s), probably because of the high electric field applied to the gate oxide, hence creating an excess of surface states (by slow trapping). The corresponding activation energy is around 1 ev.

IV. MOISTURE MEASUREMENT BY SURFACE CONDUCTIVITY SENSORS

Among several techniques available for detecting moisture in a sealed package, the surface conductivity sensors are very attractive because they allow a non-destructive, accurate and sensitive moisture measurement.

The sensor is made of an interdigited aluminum stripe pattern deposited on a thermally grown silicon oxide. As shown in Figures 1 and 2, Two different test structures have been used in this study; the main differences between these two structures are the shape and length of the aluminum electrodes, and the existence of a diode on the latest die itself, which enables more accurate temperature measurement. The sensing die is mounted in the package to be tested. The method consists of heating the package up to 100 C and maintaining this temperature for a given period of time for desorbing the moisture fixed on the cavity walls in the same conditions as in a mass spectrometer. The package is then slowly cooled down, while the inter-electrode leakage current of the biased sensor is recorded versus temperature. Figure 3 represents the response curve that can be expected for an hermetically sealed package. It has been demonstrated that the ''dew-point'' corresponds to the onset of conduction (change in slope), the temperature of which can directly be converted to moisture content in ppmv, if one knows exactly the sealing temperature and pressure.

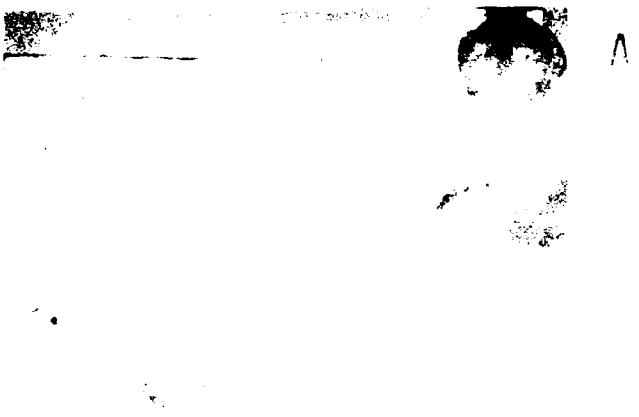

Figure 1. Interdigitated Aluminum Sensor.

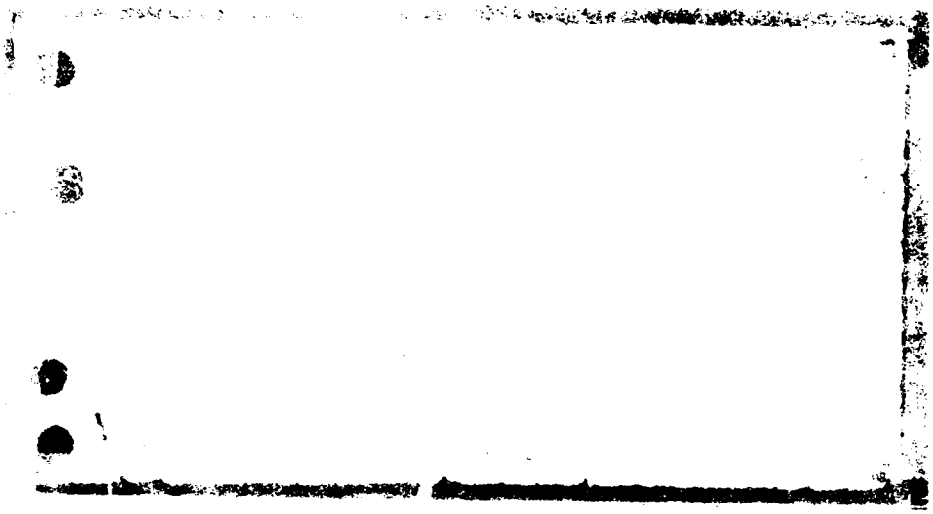

Figure 2. Interdigitated Aluminum Sensor with Diode

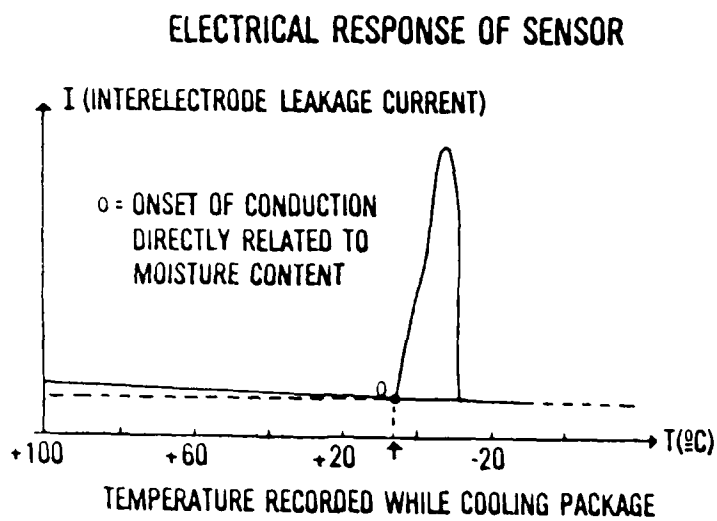

Figure 3. Expected Response Curve for an Hermetically Sealed Package

SCHEDULE OF CONDITION FOR THE TEST-SETUP CONCEPTION

* Slow and reproducible temperature scanning in the range +110C to -30C

* Coldest point at the sensor location during the cooling of the package, so that condensation occurs first on the sensor and not on the cavity walls

* A system to avoid any external condensation that could induce external leakage currents

* Possibility of generating a moisture-controlled atmosphere (known dew-point) around a biased sensor

* Accurate temperture measurement at the sensor level

* Sample holder accepting different kinds of packages

* Automated thermal cycling with adjustable temperature ramping and desorption plateau

DESCRIPTION OF THE TEST SETUP

In order to achieve the desired conditions, it was decided to put the Device Under Test (DUT) in a special test chamber. The test chamber, made of aluminum, is connected to a mechanical pump, allowing a primary vacuum (20Pa) inside the chamber. This design eliminates any possible condensation on the outside of the package, and minimizes the heat exchange with the surrounding medium. The pump is used for measurement on hermetically sealed packages only.

For calibrations and physical studies on delidded packages, the chamber also has an inlet and an outlet for gas atmospheres. The inlet is connected to the RGA calibration system at RADC, which permits a continuous flow of controlled humid gas in the chamber. The chamber has a removable top (fixed by O-ring), hermetic connectors and a power feed-through.

A schematic representation of the test chamber is given in Figures 4 and 5.

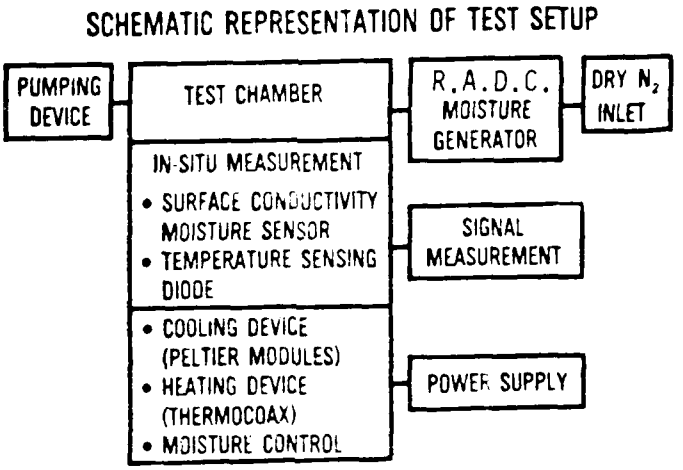

Figure 4. Schematic Representation of Test Setup

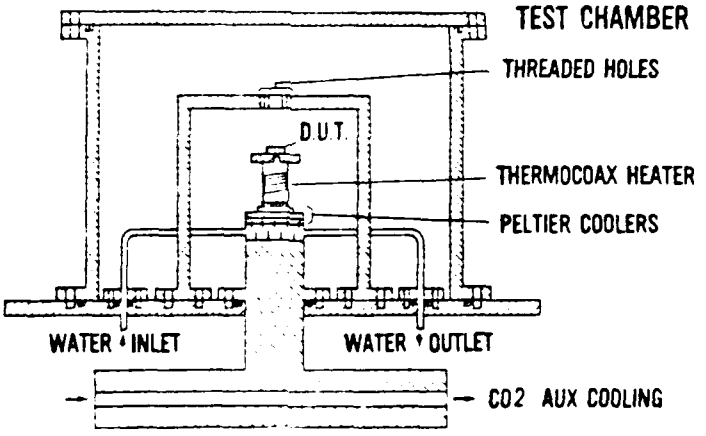

Figure 5. Diagram of Test Chamber

Thermoelectric heat pumps have have been chosen for cooling the packages. The system uses:
-one heat pump module (MELCOR CP 1.4-127-06L) biased with 11V-4A
-Three MELCOR heat pump modules in series biased with 11V-2 75A (CP 1.4 -31-06L) + (CP 1.4-71-06L) + (CP 1.4-127-06L)

Two sample holders have been designed, for use with different kinds of packages. The first one is a copper cylinder with a groove in which a thermocoaxial heater (SODERN 1 Nc Ac 20) is inserted and biased with 3V-6A. Hermetic connections (SODERN CP 20) have been welded at both ends of the heater to avoid moisture related problems. Heat from the hot surface of the heat pumps is evacuated through a water circulation box. During the experiments, circulating water has been replaced by ethylene glycol, allowing more efficient cooling. A cold finger on top of this copper piece allows a preferential cooling just underneath the sensor. This sample holder was used with TO-8 packages. An aluminum bracket with a large threaded hole on top was placed over the sample. A screw was inserted in this threaded hole. At the end of this screw, several heads could be adapted, according to the kind of device under test. These heads were made so that they could fit exactly around the top of the package to be tested. These heads have large openings on the sides, which allows a flow of gas to circulate freely around the sensor when a delidded package is being tested. A nichrome wire is wrapped around these heads and biased so that a thermal gradient of 1 to 2°C is always maintained between the top and the bottom of the DUT. This feature, together with the cold finger permit one to make sure that the sensor is always the coldest point of the package. Some TO-5 packages to be tested had an insulating glass at the bottom of the package between the leads. This glass was a very bad thermal conductor, and the previous sample holder could not be used, as too much heat was lost in the thickness of the material, which prevented from properly cooling the sample. A new sample holder was therefore designed. Its shape was a very thin copper pyramid with a three quarters of a circle long ring on top. This allowed cooling from the metal ring at the bottom side of the DUT. Moreover, some tiny holes in which the leads that were not used for the electrical measurements were inserted provided a second cooling source. As the thickness of this new sample holder did not allow the use of a thermocoaxial heater, a second nichrome wire was wrapped around the appropriate screw-head in order to heat the DUT up to 100C at the beginning of the experiments. The screw-heads also permitted retention of a good thermal contact between the DUT and the sample holder. This was improved by the presence of a thin layer of silicon grease between each surface involved in the cooling process.

ELECTRICAL MEASUREMENT CIRCUIT

Some Auger analyses have initially been performed on sensors previously biased with 40 VDC and exposed to more than 50 temperature cycles in the range +110C to -30C, in a highly humid atmosphere, which permitted:

-verifying the presence of alumina on the anode, resulting from the oxidation of the electrode after electrolysis of the adsorbed water.
-confirming the presence of aluminum on top of the silicon oxide, in the inter-electrode space.
-confirming the choice of AC bias instead of DC bias for better reproducibility in the moisture measurement.

The non-reproducibility in the electrical response of a sensor mounted in a hermetic package and exposed to thermal cycling under DC bias had been previously observed and may be explained by a variation of the silicon oxide upper layers, starting with nearly pure silicon oxide, and becoming progressively a silico-aluminate with a constantly growing proportion of alumina, reversibly changing from crystallites to gel with different time constants.

Consequently, it was decided to use a lock-in-amplifier whose internal generator would be used for biasing the DUT with a low voltage AC signal and would also be used as a reference signal. A very sensitive digital microvoltmeter was used at the output of the LIA for detecting the voltage across a resistor in series with the DUT.

Optimizing the various settings on the LIA was a necessary condition in order to reach the required sensitivity in the measurements. it implied selecting the appropriate time delay, bandwith, filters, and frequency. After many attempts, a frequency of 37.1 KHz was selected as providing the best signal to noise ratio. The choice of a high working frequency was aimed at decreasing the 1/f noise, to which the sensing device was very sensitive. The selected frequency lead to a clean signal on the recorder output of the LIA.

Figure 6 gives a schematic representation of the measurement circuit.

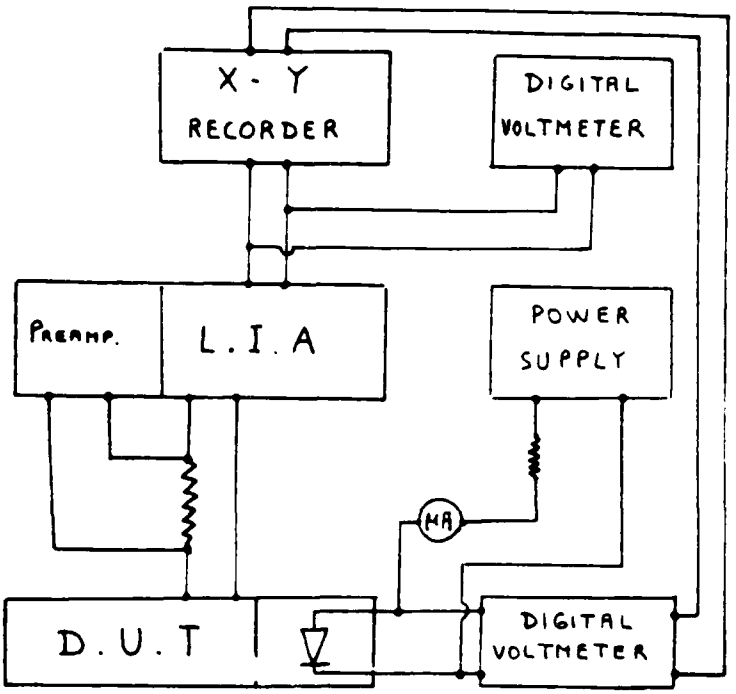

Figure 6. Schematic Representation of Measurement Circuit

AUTOMATED THERMAL CYCLING SYSTEM

For characterizing the sensors (aging, evolution of some physical parameters) an automated system has been added to the setup for performing the automated thermal cycle described in Figure 7.

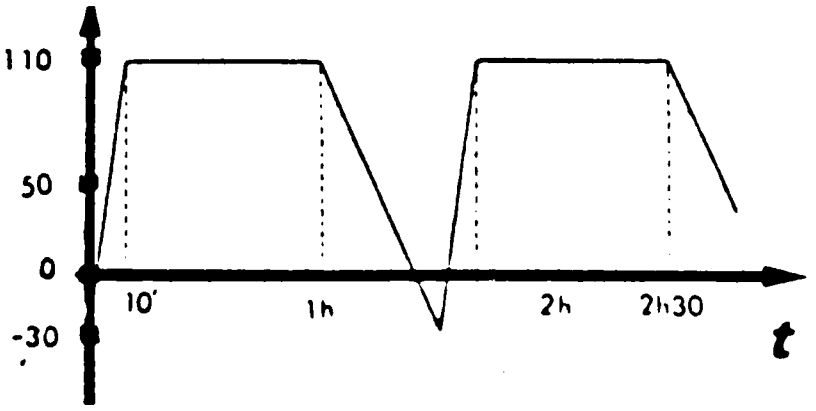

Figure 7. Automated Thermal Cycle

This system uses:
-2 temperature controllers (CHAUVIN-ARNOUX STATOP R-2SG)
-2 RTD platinum probes 100/0 C
-1 Timer on/delay-relay (CHAUVIN ARNOUX RSA 48)
-2 power relays (RSA MISS-2 Inverter/8A)

The electrical diagram of the system is given in Figure 8

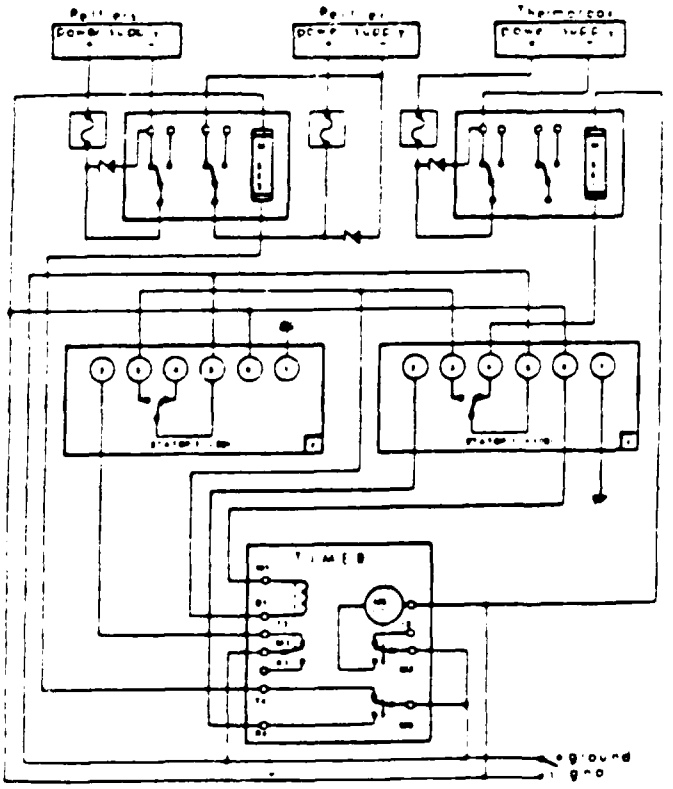

Figure 8. Electrical Diagram of the Automated Thermal Cycling System

V. EXPERIMENTAL RESULTS

Successful results were obtained with biased sensors eutectically mounted in delidded TO cans and exposed to various controlled atmospheres. These sensors were AC biased (100 mV, 37.1 KHz), initially heated up to 100°C and maintained at this temperature for several hours, and then slowly cooled down to around -30 C. The temperature was measured with a diode eutectically mounted near the sensor. A very good accuracy could therefore not be expected because of the unknown thermal gradient between the temperature sensing diode and the sensor itself. The output signal of the Lock-In-Amplifier was monitored versus temperature during the cooling of the package.

The first experiment consisted of looking at the response of a sensor exposed to the room dew-point (controlled in flow conditions by a General Eastern mirror hygrometer). An onset of conduction (change in slope) could be very clearly detected within 1.5 degrees of the room dew-point. The experiment was repeatable. Each time, the detected dew-point temperature was slightly higher than the value indicated by the hygrometer. This had also been observed previously with DC bias. It might have two causes:
-The thermal gradient in the package
-The need for a certain amount of water to be adsorbed before conduction can be electrically detected. This amount could be around three monolayers for ionic conduction, and probably a little less than one monolayer for electronic conduction. A theoretical study on conduction mechanisms in adsorbed layers between AC biased electrodes would be necessary for confirming this hypothesis.

The most important series of experiments consisted of studying the sensor response to a wide range of known dew-frost points. The test chamber was therefore connected to a gas generator that allows a flow of controlled humid gas to circulate. Several dew-frost points were generated in the range [0 C to -30 C] and the response of the sensor was recorded each time in the same conditions as for the first experiment described above. The results are summarized in Figure [illegible].

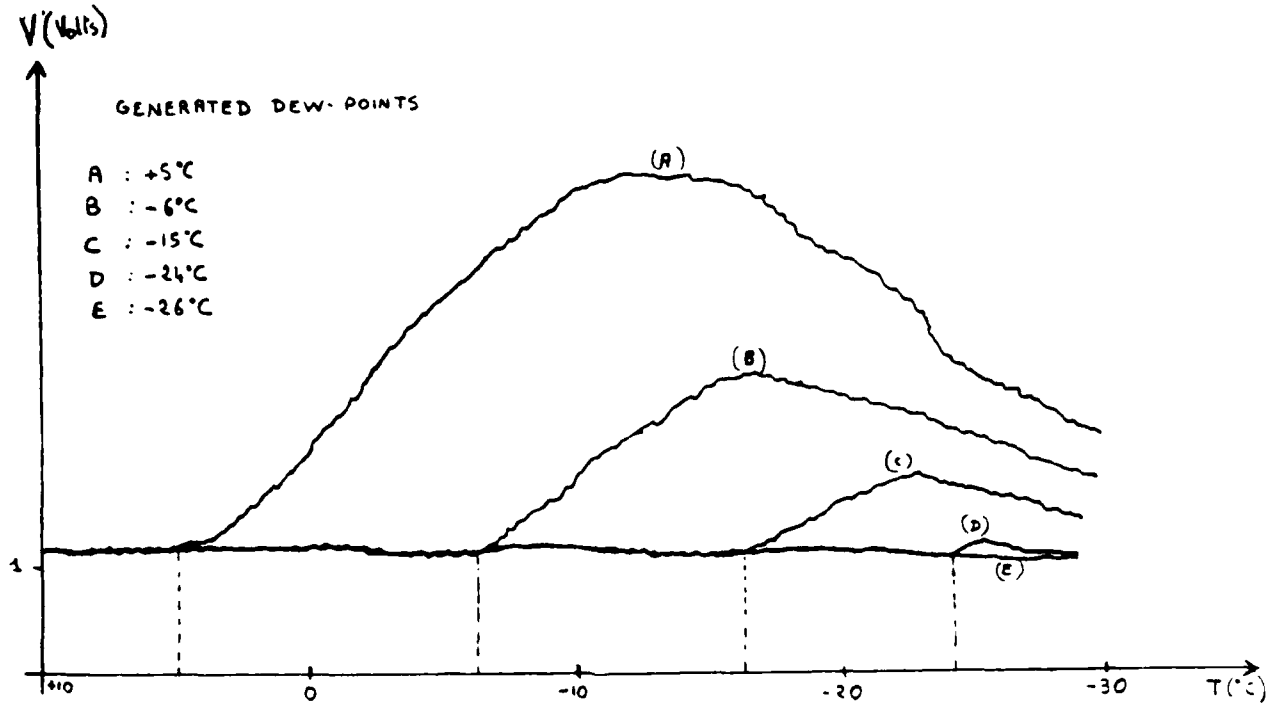

Figure 9. Dew-frost Points Sensor Responses

Several remarks can be made on this Figure:

1) The intensity of the leakage current total variation decreases with dew-frost point temperature. This means that the lower the moisture content, the lower the conduction. Therefore, the presence of water in the liquid phase and its abundance strongly affect AC conduction as it did for DC bias. This seems logical as water can be considered as a medium in which electronic and ionic conduction can occur, and as a source of ions.

2) There is an experimental limit (approximately -25 C) below which no conduction can be detected. This limit is the same as the one observed with DC bias. A physical model for explaining the existence of this limit is developed later in this report.

3) It is difficult to correlate precisely the temperature at which an onset of conduction was detected and the generated dew-point temperature because of the thermal gradient in the package. Therefore it is important to be able to measure accurately the temperature on the sensor itself, if one wants to make a quantitative measurement.

As a possible answer to this problem, 13 new sensors were sent to us (courtesy of Harris Corporation), in which a diode was integrated in the chip itself. Twelve of them passed a detailed visual inspection while 1 revealed a short between aluminum metal lines in one location. These parts were sent to Raytheon Co. for mounting (eutectic Au-Si), wire bonding and controlled sealing. The 12 ''good'' parts were divided in 4 groups of 3 devices, each group being sealed with a different moisture level (1,000 ppmv; 3,000 ppmv; 5000 ppmv and 8,000 ppmv). When the parts came back, it appeared that it was impossible to cool them down enough to reach a condensation point (the notion of dew-point is a closed package and the influence on the adsorption on the walls will be discussed later in this report), so that no measurements were possible. Some of them were open, which revealed that the dies were not properly attached. A failure analysis revealed that, even though a preform had been used, the eutectic did not stick to the die because its back surface had been previously etched. None of these dies could therefore be used, which would have given an answer to the accuracy of this measurement method.

VI. PHYSICAL MODEL FOR DETERMINING THE SENSITIVITY LIMIT

In order to assess the sensitivity limit of a surface conductivity moisture sensor, it is important to have a clear understanding of what happens to the water molecules trapped in a package cooled from +100 C to -30 C. For that purpose, Figure 10 represents the pressure-temperature diagram of water and the different phase transitions possible within this diagram.

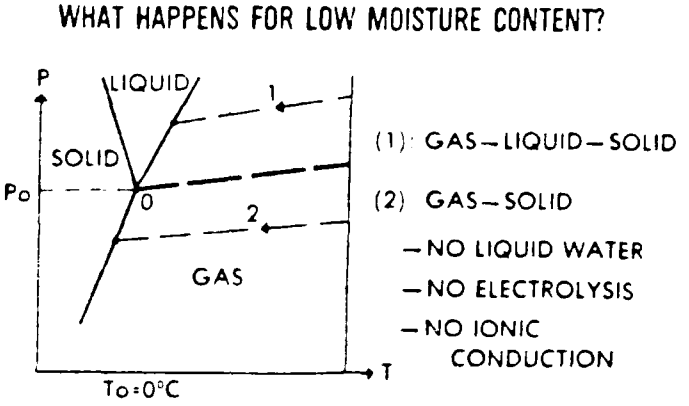

Figure 10. Pressure Temperature Diagram of Water and the Different Phase Transition

Two regions can be distinguished in this diagram:
-One region above the thick dotted line starting at the triple point O, in which Type 1 transitions can occur
-Another region below this dotted line, where type 2 transitions can occur

Once an hermetic package is sealed, it contains a fixed amount of moisture corresponding to the partial pressure of water contained in its internal atmosphere. Then, when this package is cooled, its partial pressure decreases proportionally, with a slope corresponding to the ideal gas law (P/T=cte) for a fixed volume (if one neglects the adsorption on the cavity walls, which will be taken into account in detail in the next paragraph). This is represented by the cooling lines 1 and 2 in Figure 10. Depending on the initial moisture content, the intersection between a cooling line and the phase diagram of water can be on one side or the other of the triple point, which apparently means can be either a dew point or a frost point. In the case of a dew point (type 1 transition), water vapor is first changed into liquid water, and ionic conduction can occur. In the case of a frost point (type 2 transition), there is a direct change of phase from water vapor to ice, hence neither liquid water nor ionic conduction can occur. Even electronic conduction would not be very significant.

The lowest moisture content for which a type 1 transition could theoretically occur would be around 6,500 ppmv for a metal package (sealed at 22 C) and around 14,000 ppmv for a side-brazed package (sealed at 350 C), because of the difference in their internal pressure. However, measurements have been performed with these sensors for much lower contents, and onset of conduction has been detected at temperatures below 0 C, which means that the diagram shown in Figure 10 does not represent what really happens. Some authors assume that conduction below 0 C is related to a supercooled state of water. Other authors report direct evidence of the existence of pores in dry silicon dioxide by High Resolution Transmission Electron Microscopy. The intent of the following model is to correlate the hypothesis of supercooled water to the microstructure of the silicon oxide by studying the solidification process of the water molecules that can be physisorbed in the micropores of the oxide.

The equilibrium between the three phases of water usually implies the existence of a single triple point 0. In the case of the adsorption of water on a porous material such as the silicon oxide of the sensor, water is divided, and due to capillary effects in the micropores, the equilibrium pressure and temperature of the three phases will be determined by the curvature of the menisci. Thus, when a package is cooled, the triple point temperature in the micropores will mainly depend on the curvature of the water-ice interface and therefore on the radius of this micropore.

The Gibbs-Duhem equation applied to the three phases of water at the triple point is:

$$S_l \, dT - V_l \, dP_l = 0$$

$$S_s \, dT - V_s \, dP_s = 0$$

$$S_g \, dT - V_g \, dP_g = 0$$

Where S_i is the entropy of phase i, V_i its volume and P_i its pressure. The indices 1, s, g respectively stand for liquid, solid and gas. By combining these equations, the following equation can be written:

$$\left[\left(\frac{S_s-S_g}{V_s-V_g}\right) - \left(\frac{S_l-S_s}{V_l-V_s}\right)\right]dT = \left(\frac{V_l}{V_l-V_s}\right) \cdot (dP_s-dP_l) + \left(\frac{V_g}{V_g-V_s}\right) \cdot (dP_g-dP_s)$$

According to the Gibbs model, two phases i and j with volumes V_i and V_j are separated by an interface ij whose surface is A_{ij}. The Gibbs-Duhem equation applied to the interfaces gives:

$$S_{ij} \, dT + A_{ij} \, d\gamma_{ij} + m_{ij} \, d\mu_{ij} = 0$$

where γ_{ij} is the surface tension of the interface ij and μ_{ij} its chemical potential.

According to the Laplace equation, the surface tensions are equal to:

$$\gamma_{sg} = (P_g-P_s) \cdot \frac{dV_g}{dA_{sg}}$$

$$\gamma_{ls} = (P_l-P_s) \cdot \frac{dVP}{dA_{sl}}$$

Taking these values into account, it becomes possible to write the differential equation of the triple point:

$$\left[\left(\frac{S_s-S_g}{V_s-V_g}\right) - \left(\frac{S_l-S_s}{V_l-V_s}\right)\right] dT = \frac{V_g}{V_g-V_s} \, d\left(\gamma_{sg} \frac{dA_{sg}}{dV_g}\right) - \frac{V_l}{V_l-V_s} \, d\left(\gamma_{sl} \frac{dA_{sl}}{dV_l}\right)$$

It can be seen from this equation that the triple point temperature depends only on the curvature of two interfaces (solid-gas and solid-liquid). Two other equations could be written by circular permutation of the indices.

In the case of an IC package, the volume of water adsorbed is much greater than the internal volume of the silicon oxide micropores. The gas-solid interface therefore presents no curvature and remains plane at any temperature below the usual triple point temperature 0 C, because all the water outside the micropores is transformed into ice at this temperature, which implies:

$$\frac{dA_{sg}}{dV_s} = 0$$

As $V_g >> V_l$, if $\Delta S_\gamma = S_s - S_l$ represents the solidification entropy of water, the triple point differential equation can be simplified to:

$$\Delta S_\gamma \, dT + \left(\frac{dA_{sl}}{dV_l}\right) = 0$$

This relation shows a direct correlation between the curvature of the liquid water-ice interface and the triple point temperature. The relation between this curvature and the pore radius remains to be found, which requires studying the solidification process.

Two hypothesis can be proposed for the solidification process.

-Solidification by progressive penetration of the solid phase

This process consists of a progressive penetration of the solid phase formed outside the porous material into the smaller, then the smallest micropores. The same kind of observations (shift of the triple point temperature) has been recently observed in unsaturated pores, which might invalidate this theory.

-Solidification by nucleation in the micropores

This very classical model can also be applied to the sensor. For a homogeneous liquid (non-divided), solidification occurs from critical nuclei. Embryos appear spontaneously in the liquid, but cannot grow unless they reach a minimal (''critical'') size, whose value decreases with temperature. In a porous material, the embryo is not free to reach its critical size at any temperature, as its mean radius is at most equal to the radius of the cavity in which it is. At the normal solidification temperature, the embryos cannot therefore reach their critical size in the micropores. When the temperature is lowered, solidification can occur progressively in the pores, when the size of a critical nucleus (at a given temperature) is the size of the pore.

For both of the proposed mechanisms, the curvature of the solid-liquid interface, which is assumed to be almost semi-spherical at the very moment of solidification, is $-2/R_p$ (R_p represents the average radius of the pores). The simplified differential equation of the triple point can thus be written:

$$\frac{1}{R} = \frac{1}{2\,\ell_s} \int_{T_0}^{T} \frac{\Delta SF}{V_\ell} \cdot dT$$

It is therefore necessary to know the values of ΔSF and $V_{\ell s}$ for determining the actual solidification temperature T in the pores. The triple point of water trapped in a pore can thus be represented on the pressure-temperature diagram of water by a point 0_1 lower than the usual point 0, as can be seen on Figure 11.

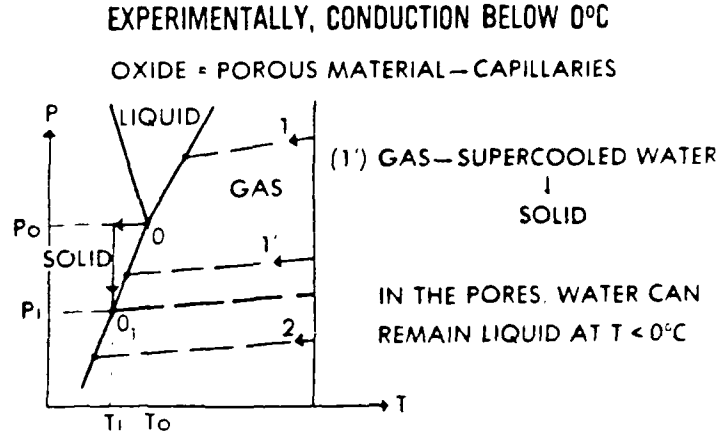

Figure 11. Triple Point for Water Trapped in a Pore

The solidification entropy is equal to the normal solidification entropy, plus the entropy along the path represented by the arrows in Figure 10 for both the liquid and solid phases.

$$\Delta S_f = \Delta S_{fo} + \left(\int_{TO}^{T} \frac{C_s}{T}\, dT + \int_{P_o}^{P_s} \frac{h_s}{T}\, dp \right)$$

$$+ \left(\int_{T}^{T_o} \frac{C_l}{T}\, dT + \int_{P_l}^{P_o} \frac{h_l}{T}\, dp \right)$$

where C_i is the specific heat capacity of phase i (at constant pressure and h_i the compression heat, defined by:

$$h_i = -T \left(\frac{\partial V_i}{\partial T} \right)_p$$

$$\Rightarrow \Delta S_f = \Delta S_{fo} + \int_{T_o}^{T} \left(\frac{C_s - C_l}{T} \right) dT + \left[\left(\frac{\partial V_l}{\partial T} \right)_p \right] (P_s - P_o) + \left[\left(\frac{\partial V_o}{\partial T} \right)_p \right] \cdot (P_l - P_s)$$

P_s is the vapor pressure of the solid at temperature T; its value is given by Clapeyron's equation. $P_l - P_s$ is given by Laplace equation.

$$P_l - P_s = \frac{2\gamma sl}{R_p} = \int_{T_o}^{T} \frac{\Delta sf}{V_l}\, dT$$

By adopting values found in the literature for ΔS_{fo}, C_s, C_l, $\left(\frac{\partial V_l}{\partial T}\right)_p$, $\left(\frac{\partial V_s}{\partial T}\right)_p$, V_l and P_o, ΔS_f can be written after approximations:

$$\Delta S_f \approx \frac{1.23 \times 10^{-1}\, T^2 + 10.13 \times 10^{-3}\, T - 4.99\, \ln\left(1 + \frac{T}{T_o}\right) - 1.22}{1 - 4.56 \times 10^{-3} (T - 0.23\, T^2)}$$

It then becomes possible to integrate the relation between the pore radius and the solidification temperature, which leads to:

$$\Delta T \approx \frac{64.7}{0.57 - R_p}$$

where $\Delta T(^{\circ}C)$ is the maximum shift of the triple point temperature of water molecules physisorbed in the micropores of the oxide, and R_p (in nm) the average radius of these pores.

This relation shows that, the smaller the pore size is, the greater the shift of the triple point temperature. Moreover, as can be seen in Figure 10, a 1' transition (water vapor to supercooled water to ice) can occur between 0 C and the actual solidification temperature in the pores allowing electrical conduction (ionic and electronic) to occur, and the sensor to work below 0 C.

According to the above relation, the experimental limit of -25 C would correspond to a pore radius of 3.5 nm. This value is higher than what has been observed by some authors by High Resolution TEM on thin thermal SiO films. However, the oxide of the sensors used in this study is thick, and presents a multilayer (dry/wet/dry) structure. Moreover, $C_2 H_3 Cl_3$ has been added to the oxidizing atmosphere for neutralizing Na and other contaminating alkali ions, hence a different microstructure exists for which no direct observation is reported in the literature. Pores 6 nm in diameter were found earlier in wafers identical to those used in these sensors, by Small Angle X-Ray Scattering (SAXS). This technique consists in recording the intensity of the diffraction obtained from a sample irradiated with X-rays (wavelength λ = 1 to 2 Angstroms) versus the incident angle θ which varies from 0 to 2 degrees. In the case of porous SiO, the sample is assumed to be a two-phase system, one of them being a SiO matrix with a high electron density, and the other, dispersed pores with a null electron density. If the absolute intensity is known, which requires a precise knowledge of the irradiated volume, it has been shown that the recorded curve is the Fourier Transform of a ''correlation function'' whose first derivative at the origin (tail of the curve) can be expressed in terms of the specific surface of the sample. The correlation function drops to zero asymptotically, showing an inverse fourth power of $h = 4\pi\lambda^{-1}\sin\theta$ for large angles. If the irradiated volume is not known precisely, it is necessary to normalize the intensity by a factor $Q = \int h^2 I(h)dh$ for determining the actual surface area of the sample. Then, one has to adopt a model for the pore size distribution (for example, cylindrical pores equally apart from one another), and to compare the theoretical and experimental scattering curves for determining an average pore radius.

VII. PHYSICAL MODEL FOR QUANTIFYING THE EFFECT OF ADSORPTION ON THE CAVITY WALLS

The concept of dew-point has often been improperly used when reporting moisture measurements by means of sensing devices for which a cooling process is necessary. This can be because one usually neglects the effect of adsorption on the cavity walls. Most tables giving a correlation between a dew point temperature and a moisture content expressed in ppmv are based on the straightforward application of the ideal gas law. The intent of this portion of the report is to develop a modified gas law model that takes into account adsorption on the cavity walls during the cooling of the package.

The ideal gas law applied to the partial pressure of water gives:

$$P V = n R T$$

Where P is the partial pressure of water, V the volume of the package, n the total number of moles, R the universal gas constant and T the temperature.

If one takes adsorption into account, this gives:

$$P V = (n_{100\,^{\circ}C} - n_{ads}) R T$$

Where n_{ads} is the number of moles adsorbed on the walls at temperature T

Assuming that nothing is adsorbed at 100°C when the cooling process starts, this allows comparisons with moisture hygrometric techniques, for which measurements are made at this temperature, and can be determined by the BET model. The BET model developed by Brunauer, Emmet and Teller is a surface multilayer adsorption model based on the assumption that the heat of adsorption of the gas is required for the adsorption of the first monolayer and that all the other adsorbed layers with an identical energy which is the heat of vaporization.

The BET model assumes that there is a permanent statistical equilibrium between the adsorbed layers which implies that a molecule evaporating from a layer i will be adsorbed on layer (i-1) at a rate proportional to the partial pressure of water in the package and to the surface involved. The equilibrium between successive layers can be expressed by:

$$a(i-1) \cdot P \cdot S_{(i-1)} = a_i \cdot S_i \cdot e^{-E_i/RT}$$

Where E_i is the energy required for one adsorbed molecule to evaporate from layer i, and $a(i-1)$, a_i are the corresponding coefficients.

As previously mentioned, the first adsorbed layer is different from the others for which interaction with the surface can be neglected.

$$V_i > 2 \quad E_i = E(i+1) = E_l \qquad \frac{a_{(i+1)}}{a_i} = g$$

All the layers whose order is greater than 1 are thus identical to a liquid, each layer being in a statistical equilibrium with the layer on which it is lying and therefore with layer 1. This explains how the upper layer can remain in equilibrium with the vapor at a pressure lower than the saturating vapor pressure.

The previous equations can be condensed to:

$$S_1 = \frac{a_0}{B_1} \cdot P \cdot s_0 \exp\left[\frac{E_1}{RT}\right]$$

$$V_i > 2, \quad S_i = \frac{1}{g} \cdot P \cdot S(i-1) \exp\left[\frac{E_l}{RT}\right]$$

Let r and q be defined by:

$$r = \frac{P}{g} \exp\left[\frac{E_l}{RT}\right]$$

$$q = \frac{a_0}{B_1} P \exp \qquad \Rightarrow C = \frac{q}{r} = \frac{a_0}{B_1} g \exp\left[\frac{E_1 - E_l}{RT}\right]$$

One can write:

$$S_i = q\, S_0$$

$$\Rightarrow S_i = r^{i-1} g\, S_0 = C\, r^i\, S_0$$

$$S_i = r^{i-1} S_1$$

The total surface of the adsorbate is:

$$S = \sum_{i=1}^{n} S_i = S_o + C\, r\, S_o + C\, r^2\, So + \ldots\ldots\ldots + C\, r^n\, S_o$$

$$\Rightarrow S = S_o \left(1 + C \sum_{i=1}^{n} r^i\right)$$

If V_o represents the volume of gas necessary to cover one surface unit with one monolayer, the total adsorbed volume can be written:

$$V = \sum_{i=1}^{n} i\, V_o\, S_i = V_o \sum_{i=1}^{n} i\, S_i = C\, S_o\, V_o \sum_{i=1}^{n} i\, r^i$$

$Vm = SV_o$ represents the volume of gas necessary to cover the entire adsorbate with one monolayer. Thus:

$$\frac{V}{V_m} = \frac{C \sum_{i=1}^{n} i\, r^i}{1 + C \sum_{i=1}^{n} r^i}$$

When the partial pressure of water gets close to the saturating vapor pressure, the adsorbed volume becomes almost infinite because the gas is liquified and covers the surface of the adsorbate with an infinite number of layers.

However, for $r < 1$, if $n \to \infty$, $\sum_{i=1}^{n} r^i = \frac{r}{1-r}$

One can also write: $\frac{d\, r^i}{dr} = i\, r^{i-1} \Rightarrow r \frac{dr^i}{dr} = i\, r^i$

which leads to: $\sum_{i=1}^{n} i\, r^i = r \sum_{i=1}^{\infty} \frac{dr^i}{dr} = r \frac{d(\sum_{i=1}^{n} r^i)}{dr} = \frac{r}{(1-r)^2}$

It is therefore obvious that:

$$\frac{V}{V_m} = \frac{Cr(1-r)^{-2}}{1 + Cr(1-r)^{-1}} = \frac{C\, r}{(1-r)\ (Cr+1-r)}$$

If $V \to \infty$, $r \to 1 \Rightarrow \frac{P_o}{g} \exp \frac{EP}{RT} \to 1$

Thus: $$r = \frac{P[H_2O]}{P^o[H_2O]}$$

r is the ratio between the saturating vapor pressure of water at a given temperature and the saturating vapor pressure of water at this temperature. It is called the relative humidity.

Let ρ be the volumie mass of water. Thus:

$$m = \rho V \qquad\qquad M_o = \rho V_m$$

Hence it becomes obvious that:

$$m = \frac{m_o\ C\ r}{(1-r)\ (1 + [C-1]r)}$$

where m is the total mass of adsorbed water, and m_o the mass of water contained in one monolayer.

Let $K = \frac{a_0}{B_i} g = \frac{a_0}{a_i} \frac{B(i+1)}{B_1} \Rightarrow C = K \exp \emptyset/RT$

$\emptyset = E_1 - E_1$ is the difference between the heat of evaporation of water and the heat of adsorption of water vapor on the adsorbate. The constant K is usually considered equal to 1. The number of adsorbed water molecules at a given temperature and relative humidity is therefore given by.

$$n = N_o \left(\frac{r}{1-r}\right) \frac{\exp(\emptyset/RT)}{1+r(-1 + \exp \emptyset/RT)}$$

were N_o is the number of moles necessary to cover the surface with one monolayer.

The modified ideal gas law that takes the adsorption of water on the package walls into account becomes:

$$\frac{P \cdot V}{R\,T} = n_{100°C} - \left[n_0\left(\frac{r}{1-r}\right) \cdot \frac{\exp\,(\phi/RT)}{1 + r(-1 + \exp \phi/RT)}\right]$$

If one assumes that water is uniformely adsorbed on all the internal surfaces in the package (which is not the actual cooling mode used on the surface conductivity sensors, for which a thermal gradient is supposed to allow condensation to occur first on the sensor), one can write (For A TO-5 package):

$$S = 2\pi R^2 + 2\pi RL = 2\pi(3.75\times10^{-3})^2 + 2\pi(3.75\times10^{-3})\,(3.5\times10^{-3}) = 1.71\times10^{-4}\ m^2$$

One molecule of water in the physicsorbed state occupies 10.2 A^{o2}

Hence, No= 2.78×10^{-8} moles

The saturating vapor pressure of water at a given temperature is given by the Clapeyron equation:

$$P^{o}[H_2O] = P_{100°C}\ \exp\left(\frac{\Delta H_{vaporization}}{R}\left[\frac{1}{373} - \frac{1}{T}\right]\right)$$

$$\text{with } P_{100°C} = P_{seal} \times \frac{373}{T_{seal}} = 1.25 \text{ atm}$$

$$\Delta H_{vap} = 2.26\ 10^6\ J/k_g = 9.73 \text{ kcal/mole}$$

$$\Rightarrow (r)_T = \frac{P}{1.25 \exp\,[4870(1/373 - 1/T]}$$

$$\text{and } N_{100°C} = \left(\frac{P \cdot V}{R\,T}\right)_{273K} = 9\times Z\times10^{-2}$$

with Z= moisture content at 100°C in ppmV

The modified ideal gas law can thus be written:

$$P = \frac{T}{1.1\times10^{-7}}\left(9\times10^{-2}Z - \left[2.78\times10^{-9} \times \frac{P}{1.25 \exp[4870(\frac{1}{393} - \frac{1}{T})]} - P \times \frac{1}{1+(-1 + \exp\frac{650}{T})(\frac{P}{1.25 \exp[4870(\frac{1}{373} - \frac{1}{T})]})}\right]\right)$$

with $\phi \approx 1.3$ Kcal/mole

This equation was solved by computer. The results are summarized in the following table. The results of this study show that when a ''dew-point'' is being electrically detected by the sensor, the actual moisture content of the package at 100 C (i.e. the expected result of an RGA measurement) is much higher than what could be computed by applying the classical ideal gas law to the partial pressure of water. This is very important if one tries to correlate results obtained by different analytical techniques. However, this model does not take into account the thermal gradient of the package, nor the possible presence of other materials in the package on/in which moisture could be adsorbed/absorbed.

TABLE I

Computer Solutions to Equation on Page 27 .

Moisture Content ppm V	Dew Point Temperature ^{o}K	Pressure LHS, ATM	Pressure RHS, ATM	P/P_o	No. of Iterations
500					
500	242.9001	1.519492E-04	4.432152E-04	.342834	119
500	243.0001	1.529584E-04	4.476917E-04	.3416602	118
500	243.1001	1.539695E-04	4.522091E-04	.3404831	117
500	243.2001	1.54982 E-04	4.567665E-04	.3393026	117
500	243.3001	1.559962E-04	4.613658E-04	.3381183	116
500	243.4001	1.570119E-04	4.660058E-04	.3369313	116
1000					
1000	247.1003	3.662973E-04	6.698946E-04	.5467985	129
1000	247.2003	3.687223E-04	6.763662E-04	.545152	128
1000	247.3003	3.711498E-04	6.828936E-04	.5434957	124
1000	247.4003	3.735782E-04	6.894771E-04	.5418283	128
1000	247.5003	3.760083E-04	6.961169E-04	.5401511	122
1000	247.6004	3.7844 E-04	7.02814 E-04	.5384639	121
3000					
3000	259.8011	1.596459E-03	2.106616E-03	.757831	130
3000	259.9011	1.605964E-03	2.124506E-03	.7559236	127
3000	260.0011	1.615452E-03	2.14253 E-03	.7539927	125
3000	260.1011	1.624918E-03	2.160689E-03	.7520373	123
3000	260.2011	1.634362E-03	2.178984E-03	.750057	122
3000	260.3011	1.643785E-03	2.197417E-03	.7480533	120
5000					
5000	266.3015	2.967829E-03	3.589697E-03	.8267631	152
5000	266.4015	2.985138E-03	3.618324E-03	.8250057	146
5000	266.5015	3.002401E-03	3.647152E-03	.823218	139
5000	266.6015	3.019618E-03	3.676182E-03	.8214004	130
5000	266.7015	3.036781E-03	3.705416E-03	.8195519	127
5000	266.8015	3.053892E-03	3.734853E-03	.817674 5	127
10000					
10000	275.9021	6.028246E-03	7.446527E-03	.809538	61

TABLE II

Dew Point for Different Moisture Content

MOISTURE CONTENT at 100 C (in ppmv)	DEW-POINT (Computed by Ideal Gas Law)	DEW-POINT (Computed by modified Ideal Gas Law)
500	-29 C	-30 C
1000	-23 C	-27 C
3000	-9 C	-13 C
5000	-3 C	-7 C
10000	+6 C	+2 C

VIII. RECOMMENDATIONS

The following recommendations can be made at the end of this study:

1) Surface conductivity moisture sensing chips can be used for performing measurements of any hermetic package moisture content provided that all the conditions listed below are fully satisfied:

   -The chip must include a temperature sensing diode

   -The die-attach material must be a good thermal conductor, and must not absorb more moisture than the other materials in the cavity.

   -AC bias is required in order to avoid reproducibility problems.

   -The bias frequency and voltage must be optimized according to the measurement circuit used. The use of a Lock-In-Amplifier is advised for obtaining the required sensitivity (signal to noise ratio).

   -A thermal gradient must be maintained in the package, so that condensation can be assumed to occur first on the sensor.

   -The adsorption properties of all the materials used in the package (plating, lid) must be known precisely, if one wants to make a quantitative measurement, and correlate this result to other techniques such as RGA, for which the thermal conditions are different.

   -A precise knowledge of the sealing conditions (temperature, pressure) is also necessary.

2) Anybody working in packaging reliability, screening, accelerated life test, failure analysis and other similar fields must be aware of the fact that the moisture trapped in any porous material can remain liquid by capillary effect, at a temperature much below 0 C and can be the origin of the failure mechanisms described in this report, provided that a ''dew-point'' temperature is reached.

IX. CONCLUSIONS

1) A new, original test setup has been developed at RADC, that allows measuring non-destructively the water vapor content of any integrated circuit hermetic package. This system allows working either in vacuum for measurements on hermetically sealed parts, or in a controlled humid atmosphere, for calibrations on delidded parts.

2) Calibrations have been successfully performed on AC biased interdigited surface conductivity moisture sensors eutectically mounted in delidded TO-5 packages, for moisture levels corresponding to the range [0 C to -25 C] in ''dew-frost'' points.

3) A physical model has been developed which demonstrates that the sensitivity limit of such sensors strongly depends on the microstructure of the oxide used in the sensor fabrication. This model shows that using an oxide with smaller pores would theoretically allow improving the sensitivity of these devices.

4) A physical model has been developed that allows correlating the electrical ''dew-point'' measured by an in-situ surface conductivity sensor to the actual moisture content as measured by a mass spectrometer. This model is a modification of the ideal gas law applied to the partial pressure of water in the package, that takes into account the adsorption on the cavity walls during the cooling process. However, the accuracy of this model would be improved if one could quantify the influence of the thermal gradient in the package.

5) Several recommendations have been made that should allow potential users of this very promising technique to be aware of its requirements and limitations.

APPENDIX

PROCEDURE FOR USING THE TEST SETUP

1) Connect the vacuum gage wire to the vacuum gage connector on the side of the chamber.

2) Connect the two wires of the heat pumps mounted in series to two wires of the feed-through. Connect the corresponding pins on the feed-through to a power supply (set on 11V, 2.75 A).

3) Connect the two wires of the single heat pump to two other wires on the feed-through. Connect the two corresponding pins to a power supply (set on 11V, 4A).

4) Connect the two wires of the thermocoaxial heater to two other wires on the feed-through, and the two corresponding pins to a power supply (set on 3V, 6A).

5) Connect the two ends of a Nichrome resistor wrapped around the appropriate head of the screw (the choice of the screw is determined by the Device Under Test, as mentioned on page 11) to the two last wires on the Feed-through. Connect the two corresponding pins to a power supply set on a voltage and a current such that a thermal gradient of 1 to 2 C is maintained between the top and the bottom of the package. The thermal gradient can be measured by placing two thermocouples respectively above and underneath the package to be tested.

6) Connect the fluid circulation box inlet and outlet (under the test chamber) to either a water arrival and a sink or, better, to a refrigeration fluid circulation unit (ethylene glycol...).

7) Deposit a thin layer of silicon grease (for instance, GE 624) between each of the heat pumps, at the bottom of the single one and on top of the smallest one.

8) Center the single heat pump on the circulation box, and make sure that the surface on which some points have been drawn (cold surface) is on top.

9) Center the three heat pumps in series on top of the previous one (smaller on top and for each of them, cold surface with points on top).

10) Set the thermocoaxial heater around the copper sample holder (in the groove, in the case of the bigger one).

11) Put the sample holder on top of the smallest heat pump.

12) Insert one of the two screws (the longer one with the smaller sample holder and vice-versa) in the threaded hole in the center of the aluminum bracket.

13) Solder 1 inch long thin wires to the appropriate leads on the package to be tested.

14) Put the package to be tested on top of the sample holder.

15) Put the appropriate head (with the nichrome wire rolled around) at the end of the screw. Prevent it from turning with one hand, while the screw is being fastened down, until the DUT is tightly held on the sample holder. Make sure that the heat pumps remain centered during this operation.

16) Connect wires 0 and 31 (inside of the connector) to the two leads corresponding to the sensor on the DUT.

17) Connect wires 6 and 7 (inside of the connector) to the two leads corresponding to the temperature sensing diode on the DUT.

18) Connect wires 18 and 19 (outside of the connector) to a power supply. A resistor must be mounted in series with the diode (outside the chamber) and the power supply must be set so that a constant current of 10 A circulates through the temperature sensing diode.

19) Connect wires 9 and 10 (outside the connector) to the input of the preamplifier (set on position "A") on the Lock-In-Amplifier (LIA). These wires correspond to the voltage across the resistor in series with the sensor.

20) Connect wires 1 and 2 (outside of the connector) to the output of the reference channel on the LIA. These wires correspond to the sensor AC bias current.

21) If the bigger sample holder is being used (which will be true for most packages except TO-5s), insert the platinum probes in the corresponding holes.

22) Connect wires 5, 6 and 7 (outside of the connector) to the inputs 9, 10 and 8 respectively on one of the temperature controllers.

23) Connect wires 2, 3 and 4 (outside of the connector) to the inputs 9, 10 and 8 respectively on the other temperature controller.

24) Connect the automated temperature cycling system according to Figure 8.

25) Set the LIA on:

- Time constant - 1 sec
- Hi-Dyn range
- Sensitivity - 1 V (signal channel)
- Band-Pass Filter = 750 Hz (signal channel)
- Q = 1
- Internal reference (reference channel)
- Frequency = 37.1 KHz (reference channel)
- Phase Shift = 6 degrees (reference channel)
- Amplitude = 0.1 V (reference channel)

26) Connect the LIA output and the recorder output of the digital voltmeter used for monitoring the temperature to an X-Y recorder as shown in Figure 6.

27) Make sure the large O-ring on top of test chamber is properly inserted in its groove. Close the chamber and tighten the eight screws.

28) Close the gas inlet valve (if connected) and the gas outlet.

29) Put the vacuum pump on.

30) After half an hour, turn on the automated thermal cycling system (if connected), and turn on the power supply corresponding to the heating thermocoax.

31) Maintain a desorption plateau between 100°C and 105°C for several hours. With the previously listed settings, provided that a good thermal contact is maintained everywhere, the system should stay at this temperature by itself.

32) Calibrate the X-Y recorder axis so that the desired temperature range can be plotted on the X axis and the desired voltage range on the Y axis. These settings depend on whether one wants to plot the entire curve or to "enlarge" an area of the curve just at the onset of conduction (which is strongly advised if one wants to make an actual measurement).

33) Turn the power supply corresponding to the thermocoaxial heater off, and the two power supplies corresponding to the heat pumps on.

34) Record the response curve while the package is being cooled down.

35) Note the temperature at which a change of slope occurs (onset of conduction) and use the modified gas law equation to determine the moisture content of the package.

MISSION
of
Rome Air Development Center

RADC plans and executes research, development, test and selected acquisition programs in support of Command, Control, Communications and Intelligence (C^3I) activities. Technical and engineering support within areas of competence is provided to ESD Program Offices (POs) and other ESD elements to perform effective acquisition of C^3I systems. The areas of technical competence include communications, command and control, battle management, information processing, surveillance sensors, intelligence data collection and handling, solid state sciences, electromagnetics, and propagation, and electronic, maintainability, and compatibility.

END

DATE

FILMED

DTIC

4/88